Modeling of InGaN/Si tandem solar cells

L. Hsu[1] and W. Walukiewicz[2,a)]
[1]*Department of Postsecondary Teaching and Learning, University of Minnesota, Minneapolis, Minnesota 55414, USA*
[2]*Electronic Materials Program, Materials Science Division, Lawrence Berkeley National Laboratory, Berkeley, California 94720, USA*

(Received 15 February 2008; accepted 30 April 2008; published online 22 July 2008)

We investigate theoretically the characteristics of monolithic InGaN/Si two-junction series-connected solar cells using the air mass 1.5 global irradiance spectrum. The addition of an InGaN junction is found to produce significant increases in the energy conversion efficiency of the solar cell over that of one-junction Si cells. Even when Si is not of high quality, such two-junction cells could achieve efficiencies high enough to be practically feasible. We also show that further, though smaller, improvements of the efficiency can be achieved by adding another junction to form an InGaN/InGaN/Si three-junction cell. © *2008 American Institute of Physics*.
[DOI: 10.1063/1.2952031]

I. INTRODUCTION

Because of the limitations in the ability of a one-junction solar cell to utilize efficiently the photons of the broad solar spectrum, multijunction solar cells have been the focus of much theoretical and experimental work in the past few decades.[1] The most successful efforts to date have concentrated on using well-known semiconductors such as Ge, InP, GaAs, GaSb, and various III-V alloys to construct such cells, achieving energy conversion efficiencies of over 30% for two-junction cells[2] and over 40% for three-junction cells combined with solar concentrators.[3]

Recent advances in the growth and doping of InGaN alloys may provide an alternative to traditional III-V materials. The bandgap of InGaN can be varied from 0.7 to 3.4 eV, making it suitable for a wide range of multijunction solar cell designs. These cells would be able to utilize high energy photons with more efficiency than those made from traditional III-V alloys, which are limited to bandgaps of less than 2.2 eV. Such cells would also have the advantage that Si is relatively cheap and plentiful and its processing techniques are well established, in addition to the fact that the Si bandgap of 1.1 eV is ideally suited for the bottom junction of a high efficiency two-junction solar cell.

InGaN/Si solar cells also have one additional benefit over those constructed from traditional III-V materials. As one can see from Fig. 1, at an alloy composition of $In_{0.46}Ga_{0.54}N$, the conduction band of InGaN has the same energy (relative to the vacuum) as the valence band of Si, and so a n-$In_{0.46}Ga_{0.54}N/p$-Si interface should form a low resistance Ohmic junction. In fact, this behavior has been observed for an n-$In_{0.4}Ga_{0.6}N/p$-Si junction.[4] Thus, a two-junction InGaN/Si tandem solar cell where the InGaN has an alloy fraction close to $In_{0.46}Ga_{0.54}N$ can be grown without heavy doping of the interface between the two materials, as is required in multijunction cells constructed from traditional III-V materials. As a bonus, the bandgaps of such a cell would be 1.1 eV (Si) and 1.8 eV ($In_{0.46}Ga_{0.54}N$), close to the bandgap combination predicted to give the maximum energy conversion efficiency for two-junction solar cells.[5,6]

In this paper, we calculate the characteristics of series-connected, monolithic, two-junction, two-terminal InGaN/Si solar cells under a variety of conditions, including those in which the semiconductor materials are of less than optimal quality. We also briefly discuss results regarding a three-junction cell, consisting of two InGaN junctions grown on Si. The fact that present cells made from conventional semiconductors have efficiencies not far from their theoretically calculated values is an encouraging sign that our results may be experimentally relevant. Significant challenges such as the poor structural quality of nitride materials remain potential obstacles to the practical development of InGaN/Si solar cells. However, because the relatively large density of structural defects has not precluded the commercial use of the nitrides in certain device applications, it remains to be seen whether the issue of good quality growth will pose an insurmountable problem in the creation and development of ni-

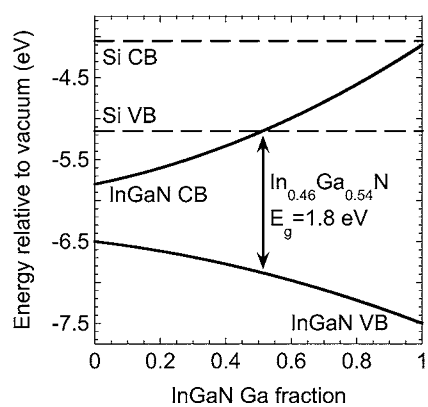

FIG. 1. Energy diagram showing the conduction and valence bands of InGaN as a function of alloy composition. The conduction and valence bands of Si are shown for comparison. At an alloy composition of $In_{0.46}Ga_{0.54}N$, the bottom of the InGaN conduction band and the top of the Si valence band have the same energy, relative to the vacuum. Thus, an n-$In_{0.46}Ga_{0.54}N/p$-Si interface forms a low resistance Ohmic junction.

a)Electronic mail: w_walukiewicz@lbl.gov.

 © 2008 American Institute of Physics

Downloaded 05 Aug 2008 to 130.236.174.80. Redistribution subject to AIP license or copyright; see http://jap.aip.org/jap/copyright.jsp

p-InGaN	$p = 5 \times 10^{17} cm^{-3}$
n-InGaN	$n = 5 \times 10^{18} cm^{-3}$
p-Si	$p = 6 \times 10^{17} cm^{-3}$
n-Si	$n = 6 \times 10^{17} cm^{-3}$

FIG. 2. Schematic diagram of the solar cell structure used in the calculations. The thickness of the InGaN junction was adjusted wherever possible to match the short circuit currents of the InGaN and Si junctions. The thicknesses of the *n*- and *p*-type layers were determined by Eq. (8).

tride solar cells. For the time being, we ignore such considerations, as our goal is to investigate whether the theoretically achievable efficiencies warrant further development work on InGaN/Si solar cells.

II. METHOD

The solar cell structure we use to model the performance of an InGaN/Si solar cell is shown in Fig. 2. The tandem cell consists of an InGaN p/n junction grown on top of a Si p/n junction. Each junction is composed of a p-type layer grown on top of an n-type layer. Within these layers, holes travel upward (toward the surface of the cell) and electrons travel downward (toward the back contact of the cell).

The calculations were performed using a modified version of the standard equations for calculating the electrical characteristics of a tandem solar cell.[5–7] Previous studies have usually assumed that all photons with energies larger than the bandgap of the cell are absorbed and converted into an electron-hole pair[6,7] and that every electron-hole pair created reaches the cell terminals.[5–7] However, because Si is an indirect gap semiconductor and the Si junction thickness needed to achieve maximum efficiency may be several times larger than the minority carrier diffusion lengths, we do not make such assumptions. Instead, our calculations of the short circuit current density explicitly include the absorption coefficients of InGaN and Si, the junction thicknesses, and the diffusion lengths. As in previous studies, we omit explicit consideration of any reflective and resistive losses in the system and assume that every photon absorbed creates one electron-hole pair.

To find the short circuit current density, we first calculate the short circuit current densities in each layer (p or n) of each junction separately. For example, to find the current density generated by the p-InGaN layer, we first find the number density of photons of a particular wavelength absorbed by a thickness dx of the p-InGaN at a depth x beneath the surface. That quantity is given by the expression

$$\begin{aligned}
&\begin{pmatrix}\text{\#incident photons}\\ \text{per unit area}\end{pmatrix}\begin{pmatrix}\text{fraction of photons}\\ \text{penetrating to depth } x\end{pmatrix}\\
&\quad\times\begin{pmatrix}\text{fraction of photons}\\ \text{absorbed by thickness } dx\end{pmatrix}\\
&\quad= I_0(\lambda)\exp(-\alpha_T(\lambda)x)(1-\exp(-\alpha_T(\lambda)dx))\\
&\quad= I_0(\lambda)\exp(-\alpha_T(\lambda)x)(1-(1-\alpha_T(\lambda)dx))\\
&\quad= I_0(\lambda)\exp(-\alpha_T(\lambda)x)\alpha_T(\lambda)dx. \qquad (1)
\end{aligned}$$

All symbols are defined in the nomenclature. Since we assume that each absorbed photon creates one electron-hole pair, this expression also gives the number density of electrons and the number density of holes generated by a thickness dx of p-InGaN at a depth x below the surface. The incident photon flux $I_0(\lambda)$ is taken from the air mass (AM) 1.5 global spectrum from the ASTM G-173–03 standard.[8]

Because the layer under consideration is p-type, we assume that all holes generated reach the surface. On the other hand, recombination processes might significantly reduce the number of electrons that reach the InGaN p/n-junction and so expression (1) must be reduced by the factor $\exp[-(x_p - x)/L_e]$ in that case (the determination of the diffusion length L_e will be discussed later). Thus, the hole current density generated by the p-InGaN layer that reaches the surface is

$$e\int_0^{x_p} I_0(\lambda)\exp(-\alpha_T(\lambda)x)\alpha_T(\lambda)dx = eI_0(\lambda)(1-\exp(-\alpha_T(\lambda)x_p)), \qquad (2)$$

and the electron current density generated by the p-InGaN layer that reaches the n-InGaN layer is

$$\begin{aligned}
&e\int_0^{x_p} I_0(\lambda)\exp(-\alpha_T(\lambda)x)\alpha_T(\lambda)\exp\left(-\frac{x_p-x}{L_e}\right)dx\\
&\quad= e\frac{I_0(\lambda)\alpha_T(\lambda)L_e}{1-\alpha_T(\lambda)L_e}\left(\exp(-\alpha_T(\lambda)x_p)-\exp\left(-\frac{x_p}{L_e}\right)\right). \qquad (3)
\end{aligned}$$

A similar calculation for the n-InGaN layer, under the assumption that recombination processes do not significantly reduce the number of electrons traversing the layer but do reduce the number of holes, gives

$$\begin{aligned}
&e\int_0^{x_n}(I_0(\lambda)\exp(-\alpha_T(\lambda)x_p))\exp(-\alpha_T(\lambda)x)\alpha_T(\lambda)\\
&\quad\times\exp\left(-\frac{x}{L_h}\right)dx\\
&\quad= e\frac{I_0(\lambda)\exp(-\alpha_T(\lambda)x_p)\alpha_T(\lambda)L_h}{1+\alpha_T(\lambda)L_h}\exp\left[-x_n\left(\alpha_T(\lambda)+\frac{1}{L_h}\right)\right] \qquad (4)
\end{aligned}$$

for the hole current density generated by the n-InGaN layer that reaches the p-InGaN layer (and consequently the surface of the cell) and

$$\begin{aligned}
&e\int_0^{x_n}(I_0(\lambda)\exp(-\alpha_T(\lambda)x_p))\exp(-\alpha_T(\lambda)x)\alpha_T(\lambda)dx\\
&\quad= e(I_0(\lambda)\exp(-\alpha_T(\lambda)x_p))(1-\exp(-\alpha_T(\lambda)x_n)) \qquad (5)
\end{aligned}$$

for the electron current density generated by the n-InGaN layer that reaches the InGaN/Si interface.

Downloaded 05 Aug 2008 to 130.236.174.80. Redistribution subject to AIP license or copyright; see http://jap.aip.org/jap/copyright.jsp

Finally, the total hole current density generated by the InGaN junction that reaches the top contact can be found by adding expressions (2) and (4) and integrating over all incident photon wavelengths,

$$e\int_0^\infty I_0(\lambda)\Bigg[(1-\exp(-\alpha_T(\lambda)x_p)) + \frac{\exp(-\alpha_T(\lambda)x_p)\alpha_T(\lambda)L_h}{1+\alpha_T(\lambda)L_h}\exp\left[-x_n\left(\alpha_T(\lambda)+\frac{1}{L_h}\right)\right]\Bigg]d\lambda. \quad (6)$$

Similarly, the total electron current density generated by the InGaN junction is obtained by adding expressions (3) and (5) and integrating over all incident photon wavelengths,

$$e\int_0^\infty I_0(\lambda)\Bigg[\exp(-\alpha_T(\lambda)x_p)(1-\exp(-\alpha_T(\lambda)x_n)) + \frac{\alpha_T(\lambda)L_e}{1-\alpha_T(\lambda)L_e}\left(\exp(-\alpha_T(\lambda)x_p)-\exp\left(-\frac{x_p}{L_e}\right)\right)\Bigg]d\lambda. \quad (7)$$

Maximum efficiency is achieved when the thicknesses of the n-InGaN and p-InGaN layers are adjusted so that the electron and hole currents are equal. However, because the effect of changing the thickness of a layer is not straightforward (increasing the thickness increases the number of photons absorbed and therefore the number of carriers generated, but a larger fraction of the carriers are then lost to recombination processes), the optimization process is nontrivial. As a simplification, we take the thicknesses of the p-InGaN and n-InGaN layers to be

$$x_p = t_T\frac{L_e}{L_h+L_e}, \quad x_n = t_T\frac{L_h}{L_h+L_e}, \quad (8)$$

so that the thicker layer is the one in which the minority carrier diffusion length is longer. The short circuit current density for the top (InGaN) junction J_{SCT} is then the smaller of the resulting electron and hole current densities [expressions (6) and (7)]. An analogous calculation gives the short circuit current density for the bottom (Si) junction J_{SCB}.

Following the work in Ref. 5, we maximized the cell efficiency by adjusting the thickness of the InGaN junction t_T, whenever possible, so that J_{SCT} and J_{SCB} differed by less than 1 $\mu A/cm^2$. When such an adjustment was not possible (for instance, if J_{SCB} was larger than J_{SCT} for any top junction thickness), the short circuit current of the two-junction cell was taken to be the smaller of J_{SCT} and J_{SCB}, and t_T was set to the value that maximized J_{SCT}. Strictly speaking, one should match the operating currents of the two junctions rather than the short circuit currents. However, this would have complicated the calculations without a significant increase in accuracy since the operating current is usually within a few percent of the short circuit current.

We note that the optical thicknesses t_T and t_B of the InGaN and Si junctions are not necessarily the same as the physical thicknesses. The most efficient solar cells are designed such that internal reflections can increase the cell's effective thickness by as much as a factor of 40.[9] In our calculations, we assume a much more modest enhancement of the effective thickness, using a factor of 4 for the Si junction (since its surface cannot be textured in the "inverted pyramids" used in very high efficiency one-junction Si solar cells) and a factor of only 1 for the InGaN junction since the structural quality of this material is expected to be poor.

The reverse saturation current density for each junction was calculated assuming uniform doping of the layers.[7] Because we aim to estimate maximum efficiencies of a tandem cell, the contributions of the space charge layer recombination current and the tunneling current were ignored, as it is in most other calculations.[5,6] The magnitude of this reverse saturation (or injected) current density is

$$J_0 = e\frac{D_e}{L_e}\frac{n_i^2}{N_A}\left(\frac{\frac{S_eL_e}{D_e}\cosh\left(\frac{x_p}{L_e}\right)+\sinh\left(\frac{x_p}{L_e}\right)}{\frac{S_eL_e}{D_e}\sinh\left(\frac{x_p}{L_e}\right)+\cosh\left(\frac{x_p}{L_e}\right)}\right) + e\frac{D_p}{L_p}\frac{n_i^2}{N_D}\left(\frac{\frac{S_hL_h}{D_h}\cosh\left(\frac{x_n}{L_h}\right)+\sinh\left(\frac{x_n}{L_h}\right)}{\frac{S_hL_h}{D_h}\sinh\left(\frac{x_n}{L_h}\right)+\cosh\left(\frac{x_n}{L_h}\right)}\right). \quad (9)$$

The intrinsic carrier concentration n_i can be calculated in the usual way using

$$n_i^2 = N_CN_V\exp\left(\frac{-E_g}{k_BT}\right), \quad (10)$$

where N_C and N_V are given by $2M_C(2\pi k_BTm_e^*/h^2)^{3/2}$ and $2M_V(2\pi k_BTm_h^*/h^2)^{3/2}$, respectively.

The diffusion constants D_e and D_h can be calculated from the Einstein relationships

$$D_e = \frac{k_BT}{e}\mu_e \quad \text{and} \quad D_h = \frac{k_BT}{e}\mu_h. \quad (11)$$

The diffusion constants and the diffusion lengths L_e and L_h are related by $L_e=\sqrt{\tau_eD_e}$ and $L_h=\sqrt{\tau_hD_h}$, where the minority carrier lifetimes τ_e and τ_h are given by

$$\frac{1}{\tau_e} = \frac{1}{\tau_{SRH}} + BN_A \quad \text{and} \quad \frac{1}{\tau_h} = \frac{1}{\tau_{SRH}} + BN_D. \quad (12)$$

The voltage of a two-junction cell under normal operating conditions is simply the sum of the voltages of the individual junctions,

$$V = \frac{k_BT}{e}\left(\ln\left(\frac{J+J_{SCT}}{J_{0T}}+1\right)+\ln\left(\frac{J+J_{SCB}}{J_{0B}}+1\right)\right). \quad (13)$$

The maximum power per unit area that the cell can produce is calculated by finding the voltage and current density that maximize the product JV, found by setting its derivative equal to zero,

$$\left(\frac{d(JV)}{dJ}\right)_{J=J_{max}} = 0. \quad (14)$$

The efficiency of the cell is equal to the ratio of this maximum power to the power incident on the cell calculated directly from the solar spectrum (1000 W/m^2 for the AM 1.5 global spectrum).

Downloaded 05 Aug 2008 to 130.236.174.80. Redistribution subject to AIP license or copyright; see http://jap.aip.org/jap/copyright.jsp

TABLE I. Material parameters used in the solar cell efficiency calculations. The values for high quality Si are taken from standard references except for τ_{SRH}, which is a generic value (see Ref. 5). The effective masses are density of state effective masses. Values for high quality InGaN are taken from the literature except for τ_{SRH} and B, which are generic values (see Ref. 5). Values for low quality material are obtained as described in the text.

Parameter	Si (high quality)	Si (low quality)	InGaN (high quality)	InGaN (low quality)
M_c	6	6	1	1
M_v	1	1	1	1
μ_e (cm^2/V s)	1400	700	300	300
μ_h (cm^2/V s)	450	225	50	50
m_e^*/m_e	0.36	0.36	0.07	0.07
m_h^*/m_h	0.81	0.81	0.7	0.7
τ_{SRH}	10^{-5}	5×10^{-6}	10^{-5}	10^{-5}
B (cm^3/s)	4.73×10^{-15} [a]	4.73×10^{-15} [a]	7.5×10^{-10}	7.5×10^{-10}
S_h (cm/s)	0	10^6	0	10^6
S_e (cm/s)	0	10^6	0	10^6

[a]Reference 10

Table I shows the values of the material parameters used in our calculations. A few of the parameters, such as the band-to-band recombination coefficient and the Shockley–Read–Hall scattering time, are poorly known. In those cases, we have used the generic values found in Ref. 5. In the Si case, the "high quality" parameters along with an optical enhancement factor of 12 predict an energy conversion efficiency of 25.8% for a 10 μm thick one-junction Si cell, close to the record observed efficiency of 24.7%.[2] For InGaN, the high quality parameters give a short circuit current and open circuit voltage close to the ones reported for an InGaN/GaN solar cell as described in Ref. 11. Because of the uncertainties in the parameters and the factors ignored in the assumptions, we do not attempt to match the real-world operating characteristics closely, instead aiming only for reasonable agreement. For those same reasons and because of the difficulty in making it quantitative, we also have not attempted to account for the effect that passivation of the Si interfaces would have on the open circuit voltage of the cell.

To obtain the parameters for "low quality" Si, such as that used in commercial Si solar cells that are not single crystals, we arbitrarily reduced the electron and hole mobilities and the Shockley–Read–Hall recombination time by a factor of 2. Surface recombination velocities of reasonable magnitudes (Ref. 7, p. 15) were then chosen so that our calculations, using an optical enhancement factor of 2, predict an efficiency of 17.0% for a 20 μm thick Si cell, similar to the efficiency of commercially available one-junction multicrystalline Si solar cells. Because the structural quality of currently grown InGaN is invariably quite poor, the only difference between high quality and low quality InGaN is the surface recombination velocities, which again were chosen to have a reasonable order of magnitude (Ref. 7, p. 15).

The absorption coefficients for InGaN and Si were obtained by fitting a function to published absorption curves for each material. The absorption coefficient used for Si was

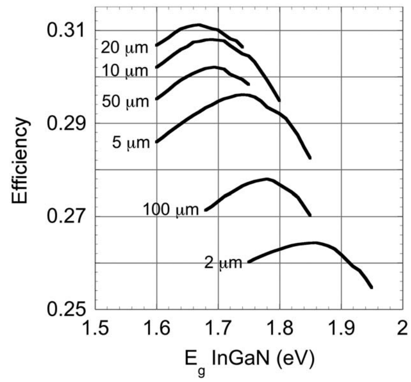

FIG. 3. Efficiency of high quality InGaN/Si two-junction solar cells as a function of InGaN bandgap. The label for each curve refers to the physical thickness of the Si junction in the cell. The effective optical thickness of the Si junction was taken to be four times larger than the physical thickness.

$$\alpha(\mu\mathrm{m}^{-1}) = -0.425(E-E_g)^3 + 0.757(E-E_g)^2 - 0.0224(E - E_g) + 10^{-4} \quad (1.1\ \mathrm{eV} < E < 1.5\ \mathrm{eV})$$
$$= 0.0287\exp[2.72(E-E_g)] \quad (E > 1.5\ \mathrm{eV}), \qquad (15)$$

using the absorption curve in Ref. 12. The absorption coefficient used for InGaN was

$$\alpha(\mu\mathrm{m}^{-1}) = 7.91(E-E_g)^4 - 14.9(E-E_g)^3 + 5.32(E - E_g)^2 + 9.61(E-E_g) + 1.98 \quad (E > E_g), \qquad (16)$$

using the absorption curve in Ref. 13. For simplicity, we ignored any effects of the InGaN alloy composition on the shape of the absorption curve (changing only the value of the bandgap E_g). Although this is not strictly correct, the error introduced by this simplification is likely to be smaller than the errors from the uncertainty in the other InGaN material parameters.

III. RESULTS

Figure 3 shows the efficiency of a tandem InGaN/Si solar cell as a function of InGaN bandgap for different Si junction thicknesses. As stated previously, the thickness of the InGaN junction was chosen to match the short circuit currents of both cells, thereby maximizing the efficiency. The material parameters used for Si and InGaN in this calculation are those from the high quality columns in Table I. The slight bumpiness in the curves shown in Fig. 3 is due to the irregularity of the AM 1.5 spectrum, which includes dips in intensity due to atmospheric absorption lines. As the bandgap of the InGaN junction is changed, the rate at which additional photons become available or unavailable for absorption changes in an irregular fashion, leading to a waviness in the curves.

As might be expected, the optimal InGaN bandgap, and consequently the InGaN alloy fraction, depends on the thickness of the Si junction. Recall that maximum efficiency is achieved when the operating currents of the InGaN and Si junctions are matched. As the Si thickness increases up to 20 μm, its short circuit current density increases because it absorbs a larger fraction of the photons with energies larger

Downloaded 05 Aug 2008 to 130.236.174.80. Redistribution subject to AIP license or copyright; see http://jap.aip.org/jap/copyright.jsp

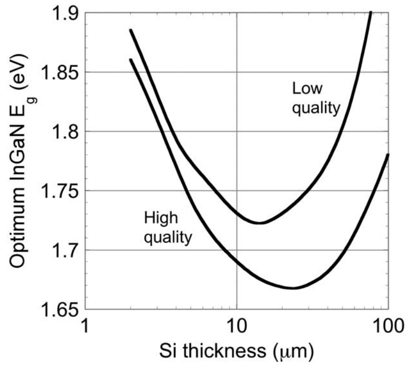

FIG. 4. Plot of the optimal InGaN bandgap for an InGaN/Si two-junction solar cell as a function of the physical thickness of the Si junction. The effective optical thickness of the Si junction was taken to be four times larger than the physical thickness.

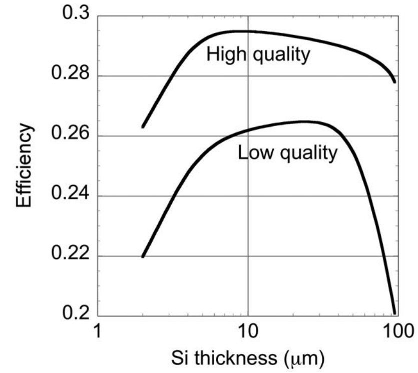

FIG. 6. Plot of the maximum efficiencies of an $In_{0.46}Ga_{0.54}N/Si$ two-junction solar cell as a function of the physical thickness of the Si junction.

than 1.1 eV. Therefore, one must decrease the bandgap of the InGaN junction so that it also absorbs more photons. As the Si thickness becomes larger than 20 μm, however, the short circuit current density of the Si junction decreases due to the loss of carriers through recombination and thermalization and the optimal InGaN bandgap increases in order to let more photons through the InGaN junction to be absorbed by Si to compensate.

Figure 4 shows the optimal InGaN bandgap as a function of the physical thickness of the Si junction. Results where both the Si and InGaN are of high quality and low quality are shown. Figure 5 shows the energy conversion efficiencies corresponding to the InGaN bandgap/Si-thickness combinations plotted in Fig. 4. The predicted efficiencies using high quality material are comparable to those of two-junction solar cells made from high quality traditional III-V semiconductors such as GaInP and GaAs. Because the material parameters corresponding to high quality InGaN reflect that of currently grown InGaN, there is a reason to believe that the expected efficiencies might climb even higher as growth techniques for III-nitride alloys improve.

While the calculated energy conversion efficiencies for low quality InGaN/Si two-junction cells are several percentage points lower than those for high quality cells, the maximum efficiencies are still nearly 10 percentage points higher

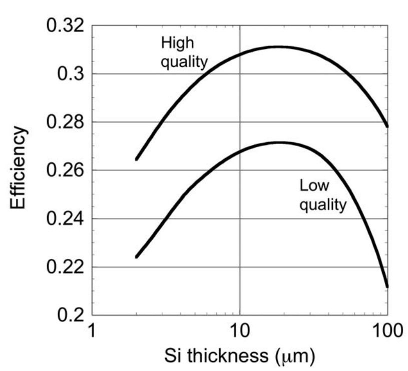

FIG. 5. Plot of the maximum efficiencies of InGaN/Si two-junction solar cells as a function of the physical thickness of the Si junction. The alloy composition of the InGaN junction was taken to be the one that maximizes the cell's efficiency, as shown in Fig. 4. The effective optical thickness of the Si junction was taken to be four times larger than the physical thickness.

than the efficiencies of commercial one-junction Si solar cells (the maximum efficiency of a low quality one-junction Si solar cell is 17.0% using our calculations). The simple addition of a thin layer of InGaN increases the energy conversion efficiency of the cell by more than 50%. Although the InGaN/Si tandem cell has a short circuit current much smaller than that of the bare one-junction Si cell ($16\ mA/cm^2$ vs $40\ mA/cm^2$), the much larger bandgap of InGaN gives this cell an open circuit voltage almost four times larger than that of the simple Si cell (1.9 V vs 0.53 V). In addition, the fill factor of the tandem cell is roughly 10% better than that of the single junction Si cell (88% vs 81%). Although series resistances and reflective losses have not been explicitly incorporated into this calculation, such losses are partially accounted for implicitly since the values used in our calculations give results that are close to those measured for real-world devices. Our results suggest that even in nonideal situations, significant gains could be achieved by the addition of an InGaN junction to one-junction Si solar cells.

As mentioned previously, one of the advantages of the InGaN/Si combination is that for a certain InGaN alloy fraction ($In_{0.46}Ga_{0.54}N$, $E_g = 1.8$ eV), the InGaN conduction band and Si valence band line up, eliminating the need for a heavily doped interface in order to produce a low resistance Ohmic junction between the two materials. However, moving away from this particular InGaN alloy composition increases the resistance and a different solution is necessary to produce a heterojunction with an acceptably low resistance. Furthermore, it is evident from Fig. 4 that the InGaN alloy fraction that produces a low resistance junction is significantly different from the InGaN alloy fraction that is predicted to maximize the energy conversion efficiency of the cell. Figure 6 shows the efficiencies that could be expected from an $In_{0.46}Ga_{0.54}N/Si$ tandem cell. The maximum predicted efficiencies in this case are only a few percentage points lower than those obtained by choosing InGaN alloys to optimize the energy conversion efficiency, 29.4% vs 31% for high quality material and 26.4% vs 27% for low quality material.

Figure 7 shows the calculated voltage-current and voltage-efficiency curves for an $In_{0.46}Ga_{0.54}N/Si$ tandem cell made from low quality material. The *IV* curve looks reasonably good even given the low quality of the materials used. Because the conversion efficiency of the cell is a sharp func-

Downloaded 05 Aug 2008 to 130.236.174.80. Redistribution subject to AIP license or copyright; see http://jap.aip.org/jap/copyright.jsp

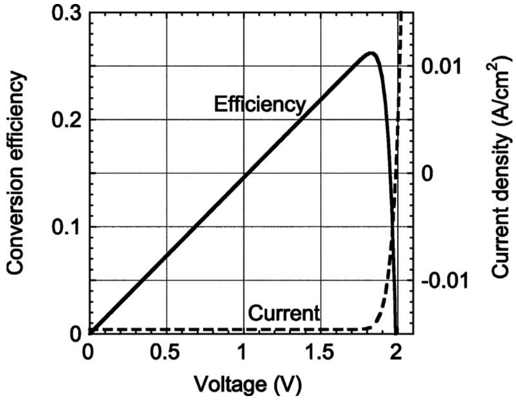

FIG. 7. Plot of the conversion efficiency (solid line) and current density (dashed line) vs operating voltage for a "low quality" $In_{0.46}Ga_{0.54}N$/Si two-junction solar cell.

tion of the voltage, care must be taken to keep the operating voltage close to its optimum value for peak performance. The optimum value of the operating voltage corresponds to a current that is about 99% of the short circuit current.

As with other multijunction solar cells such as the InGaP/GaAs or InGaP/GaAs/Ge, the increased costs of fabrication make InGaN/Si cells most practical when used in conjunction with light concentrating systems. Figure 8 shows calculated efficiencies of some tandem InGaN/Si cells under a 500 times concentration of the AM 1.5 global spectrum. At room temperature, a 500 times concentration of the incident radiation increases the efficiency of such cells by 5%–6%. However, because such concentrations of sunlight are also likely to raise the cell's operating temperature, we have also calculated efficiencies at temperatures up to 200 °C, taking into account only the increase in the reverse saturation current and ignoring the temperature dependence of the material parameters. The loss in efficiency shown occurs primarily through a reduction of the cell's operating voltage due to an increase in J_0 of nearly eight orders of magnitude over the temperature range shown. In fact, Fig. 8 likely underestimates the reduction in efficiency because the InGaN and Si bandgaps decrease with temperature, increasing the intrinsic carrier concentration (causing J_0 to increase further) and de-

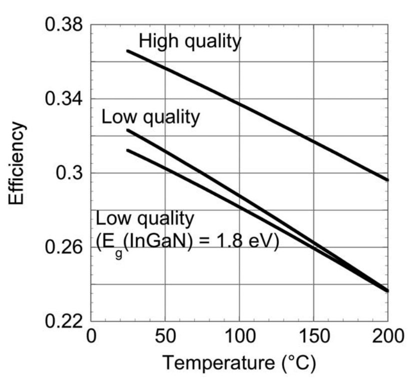

FIG. 8. Plot of the efficiencies of InGaN/Si two-junction solar cells as a function of cell temperature under 500 times concentration of the AM 1.5 global solar spectrum. The cell thicknesses were taken to be those that maximized the calculated efficiencies for each type of material (high or low quality).

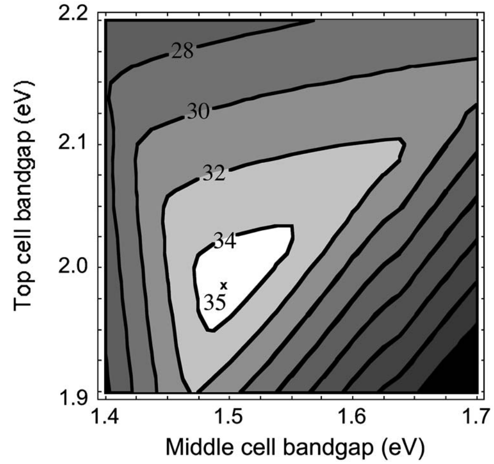

FIG. 9. Isoefficiency plot of an InGaN/InGaN/Si three-junction solar cell as a function of the bandgaps of the two InGaN junctions. The thickness of the Si junction is 20 μm. The thicknesses of the InGaN junctions were taken to be those that maximized the short circuit currents of the corresponding one-junction InGaN solar cells.

creasing the cell voltage. These results indicate that even a modest increase in the cell temperature has a considerable detrimental effect on the cell performance. Therefore good heat sinking of such cells is necessary for maintaining a high energy conversion efficiency when using concentrating optics.

Finally, we consider the efficiencies achievable by three-junction InGaN/InGaN/Si solar cells where the two InGaN junctions have different alloy compositions and bandgaps. Figure 9 shows the efficiency of such a solar cell, where the Si layer is 20 μm thick and the two InGaN junctions have thicknesses that produce the maximum short circuit current density for the corresponding one-junction InGaN cells. The use of high quality Si and InGaN was assumed. Because of the nonmonotonic relationship between the thickness of the junctions and their short circuit currents, the three-junction cells represented in the figure are not optimized for maximum energy conversion efficiency. However, the calculated maximum efficiency of 35% puts a lower bound on the true maximum value. The improvement in efficiency achieved by adding two InGaN junctions to Si as opposed to one (31%–35%) is smaller than the improvement from adding a single InGaN junction to a bare Si solar cell (25%–31%). However, for a three-junction cell, 1.1 eV is no longer the optimal bandgap for the bottom junction.

IV. CONCLUSION

We have investigated theoretically the possible energy conversion efficiencies that might be achieved by growing an InGaN junction on top of a conventional one-junction Si solar cell. InGaN is an appealing candidate to be paired with Si in a tandem solar cell not only because the bandgaps of the upper and lower cells can then be set to the values for which the theoretical maximum energy conversion efficiency would be achieved for a two-junction solar cell, but also because the alignment of the Si valence band with the $In_{0.46}Ga_{0.54}N$ conduction band eliminates the need for heavy doping at the InGaN/Si heterointerface for cells using InGaN

Downloaded 05 Aug 2008 to 130.236.174.80. Redistribution subject to AIP license or copyright; see http://jap.aip.org/jap/copyright.jsp

near that alloy composition. However, the generally poor structural quality of epitaxial layers of InGaN and of nitride materials in general poses a potential problem to the practical construction of such devices.

We have found that two-junction InGaN/Si solar cells can have significantly higher efficiencies than one-junction Si solar cells, with energy conversion efficiencies of slightly more than 31%. Even more impressive and perhaps surprising is the gain achievable with multicrystalline or otherwise low quality Si. In such cases, adding an InGaN junction on top of Si can result in increases in the energy conversion efficiencies of more than 50% compared to Si alone (27% vs 17%). Such an increase in the efficiency could justify the economic cost associated with the increased complexity of growing such cells.

The performance of InGaN/Si tandem cells under a 500 times concentrated AM 1.5 global solar spectrum is similarly impressive, with predicted efficiencies higher than 36% with high quality material. However, because the efficiency rapidly declines with temperature, careful heat sinking of such cells is critical. Finally, adding a second InGaN junction with an appropriate alloy composition can provide further boosts to the efficiency. A three-junction InGaN/InGaN/Si solar cell could offer energy conversion efficiencies in excess of 35%.

List of Symbols

$\alpha_B(\lambda)$ $\alpha_T(\lambda)$	Absorption coefficient of bottom, top junction material
B	Band-to-band recombination coefficient
D_e D_h	Diffusion constant of minority electrons, holes
E_g	Bandgap
e	Electron charge
h	Planck's constant
$I_0(\lambda)$	Incident photon flux (number density)
J	Current density
J_{0B} J_{0T}	Reverse saturation current density of bottom, top junction
J_{SCB} J_{SCT}	Short circuit current density of bottom, top junction
k_B	Boltzmann's constant
L_e L_h	Minority carrier diffusion length (electrons and holes)
M_C M_V	Number of equivalent minima in the conduction, valence band
m_e^* m_h^*	Effective mass of electron, hole
μ_e μ_h	Mobility of electrons, holes
N_A N_D	Doping concentration of p-, n-type layer of junction
N_C N_V	Density of states in the conduction, valence band
n_i	Intrinsic carrier concentration
S_e S_h	Surface recombination velocity of minority electrons, holes
T	Temperature
t_B t_T	Optical thickness of bottom, top junction
τ_e τ_h	Lifetime of minority electrons, holes
τ_{SRH}	Shockley-Read-Hall lifetime
V	Voltage
V_{OC}	Open circuit voltage
x_n x_p	Thickness of n-, p-type layer of junction

[1] J. M. Olson, D. J. Friedman, and S. R. Kurtz, in *Handbook of Photovoltaic Science and Engineering*, edited by A. Luque and S. Hegedus (Wiley, Hoboken, NJ, 2002), p. 359.
[2] M. A. Green, K. Emery, Y. Hisikawa, and W. Warta, Prog. Photovoltaics **16**, 61 (2008).
[3] R. R. King, D. C. Law, K. M. Edmonson, C. M. Fetzer, G. S. Kinsey, H. Yoon, R. A. Sherif, and N. H. Karam, Appl. Phys. Lett. **90**, 183516 (2007).
[4] J. W. Ager, L. A. Reichertz, D. Yamaguchi, L. Hsu, R. E. Jones, K. M. Yu, W. Walukiewicz, and W. J. Schaff, Proceedings of the 22nd European Photovoltaic Solar Energy Conference (WIP-Renewable Energies, Munich, Germany, 2007), p. 215.
[5] S. R. Kurtz, P. Faine, and J. M. Olson, J. Appl. Phys. **68**, 1890 (1990).
[6] M. E. Nell and A. M. Barnett, IEEE Trans. Electron Devices **34**, 257 (1987).
[7] H. J. Hovel, in *Solar Cells*, Semiconductors and Semimetals Vol. 11, edited by A. C. Beer and R. K. Willardson (Academic, New York, 1976).
[8] NREL (http://rredc.nrel.gov/solar/spectra/am1.5/).
[9] J. Zhao, A. Wang, M. A. Green, and F. Ferrazza, Appl. Phys. Lett. **73**, 1991 (1998).
[10] T. Trupke, M. A. Green, P. Würfel, P. P. Altermatt, A. Wang, J. Zhao, and R. Corkish, J. Appl. Phys. **94**, 4930 (2003).
[11] O. Jani, C. Honsberg, Y. Huang, J. Song, I. Ferguson, G. Namkoong, E. Trybus, A. Doolittle, and S. Kurtz, Conference Record of the 2006 IEEE Fourth World Conference on Photovoltaic Energy Conversion (IEEE, New York, 2006), p. 20.
[12] W. C. Dash and R. Newman, Phys. Rev. **99**, 1151 (1955).
[13] W. Walukiewicz, J. W. Ager III, K. M. Yu, Z. Liliental-Weber, J. Wu, S. X. Li, R. E. Jones, and J. D. Denlinger, J. Phys. D **39**, R83 (2006).

Downloaded 05 Aug 2008 to 130.236.174.80. Redistribution subject to AIP license or copyright; see http://jap.aip.org/jap/copyright.jsp